Received: 1 June 2022 | Revised: 12 September 2022 | Accepted: 26 September 2022

DOI: 10.1096/fj.202200848R

THE FASEB JOURNAL

RESEARCH ARTICLE

Pyruvate prevents the onset of the cachectic features and metabolic alterations in myotubes downregulating STAT3 signaling

Michele Mannelli[1] | **Tania Gamberi**[1] | **Rachele Garella**[2] | **Francesca Magherini**[1] | **Roberta Squecco**[2] | **Tania Fiaschi**[1]

[1]Dipartimento di Scienze Biomediche, Sperimentali e Cliniche "Mario Serio", Università degli Studi di Firenze, Florence, Italy

[2]Dipartimento di Medicina Sperimentale e Clinica, Università degli Studi di Firenze, Florence, Italy

Correspondence
Tania Fiaschi, Dipartimento di Scienze Biomediche, Sperimentali e Cliniche "Mario Serio", Università degli Studi di Firenze, viale Morgagni 50, 50134 Florence, Italy.
Email: tania.fiaschi@unifi.it

Funding information
Ministero dell'Istruzione, dell'Università e della Ricerca (MIUR), Grant/Award Number: RICATEN

Abstract

Cachexia is a systemic disease associated with several pathologies, including cancer, that leads to excessive weight loss due to enhanced protein degradation. Previously, we showed that cachectic features in myotubes are provoked by a metabolic shift toward lactic fermentation. Our previous results led us to hyphotesise that increasing pyruvate concentration could impede the metabolic modifications responsible for induction of cachexia in myotubes. Here, we demonstrated that the addition of sodium pyruvate in conditioned media from CT26 colon cancer cells (CM CT26) prevents the onset of either phenotypic and metabolic cachectic features. Myotubes treated with CM CT26 containing sodium pyruvate show a phenotype similar to the healthy counterpart and display lactate production, oxygen consumption, and pyruvate dehydrogenase activity as control myotubes. The use of the Mitochondrial Pyruvate Carrier inhibitor UK5099, highlights the importance of mitochondrial pyruvate amount in the prevention of cachexia. Indeed, UK5099-treated myotubes show cachectic features as those observed in myotubes treated with CM CT26. Finally, we found that sodium pyruvate is able to decrease STAT3 phosphorylation level, a signaling pathway involved in the induction of cachexia in myotubes. Collectively, our results show that cachexia in myotubes could be prevented by the utilization of sodium pyruvate which impedes the metabolic modifications responsible for the acquisition of the cachectic features.

KEYWORDS

cancer cachexia, metabolism, pyruvate

Abbreviations: CM, conditioned medium; MHC, Myosin Heavy Chain; MPC, Mitochondrial Pyruvate Carrier; OCR, oxygen consumption rate.PDH, Pyruvate Dehydrogenase; STAT3, Signal Transducer and Activator of Transcription 3; Cm, membrane Capacitance; Rm, membrane Resistance.

1 | INTRODUCTION

Cancer cachexia is a devastating and systemic syndrome that appears, although at a different levels, in the majority of cancer patients. A great disadvantage of cancer cachexia is the diminished response to anticancer treatments, associated with the worsening of the quality of life.[1,2] In skeletal muscle, cachexia induces profound phenotypic and metabolic changes that lead to pronounced weight loss. Decreased mass in cachectic muscles is mainly due to unbalanced pathways of protein synthesis and degradation, in which the ubiquitin-proteasome system and the autophagy-lysosome pathway are greatly involved.[3,4] Particularly, protein degradation is accomplished with the increased expression of the muscle-specific E3 ubiquitin ligases, such as Muscle-Atrophy-F-box (MAFbx/Atrogin-1) and muscle-RING finger-1 (MuRF1).[5] Weight loss is associated with several metabolic alterations such as enhanced glucose demand, and depleted glycogen deposits. Moreover, a reduction in pyruvate dehydrogenase (PDH) and succinate dehydrogenase (SDH) enzymatic activities was reported in cachectic skeletal muscles.[6]

Pyruvate plays a key role in glucose metabolism. In aerobic conditions, pyruvate produced by glycolysis is driven into mitochondria through the mitochondrial pyruvate carrier (MPC) and transformed in Acetyl-Coenzyme A (Acetyl-CoA) by the Pyruvate Dehydrogenase Complex (PDC).[7] Acetyl-CoA is then used in the Krebs cycle. Pyruvate dehydrogenase, one of the three components of PDC, shows decreased activity in cachectic muscle compared to the healthy one,[8] thus underlining the key role of this enzyme in cachexia onset.

Several molecular pathways contribute to muscle growth and wasting processes. Among them, the Signal Transducer and Activator of Transcription 3 (STAT3) signaling cascade is noteworthy. A number of stimuli is able to induce STAT3 phosphorylation/activation. Upon activation, STAT3 dimerizes and translocates in the nucleus to transcribe target genes. Activated STAT3 promotes skeletal muscle atrophy in muscle diseases, as shown in Duchenne muscular dystrophy (DMD),[9] and Merosin-deficient congenital muscular dystrophy (MDC1A).[11] STAT3 cascade was proven to be greatly involved in cancer cachexia,[10] as observed in muscle wasting in pancreatic tumour-bearing mice.[12] In addition, in vitro studies, where myotubes were treated with Lewis lung carcinoma conditioned medium, reported that STAT3 phosphorylation is associated with myosin heavy chain loss and muscle atrophy.[13] Moreover, STAT3 cascade was also demonstrated to drive muscle wasting induced by Interferon-gamma and tumour necrosis factor alpha through NF-*k*B.[14]

Recently, we demonstrated that cachexia onset in myotubes is associated with a metabolic change toward lactic fermentation in aerobic conditions. In this state, myotubes behave as cancer cells and can be considered "cancer myotubes." The block of the metabolic alteration, by inhibiting glycolysis with 2-deoxy-glucose or lactic dehydrogenase activity with oxamate, prevents metabolic modification and the acquisition of the cachectic phenotype.[15] Cachectic myotubes enhance lactate production and decrease oxygen consumption compared to the healthy counterpart, thus driving the majority of pyruvate produced by glycolysis toward lactate formation. On that account, we speculate that the cachectic features, acquired by myotubes treated with CM CT26, could be hampered by increasing intracellular pyruvate concentration. In this paper, we report that the addition of sodium pyruvate to CM CT26 really prevents the induction of either phenotypic or metabolic cachectic characteristics in myotubes.

2 | MATERIALS AND METHODS

2.1 | Materials

Murine C2C12 myoblasts were from ECACC. The murine CT26 colon carcinoma cell line was purchased from ATCC. Unless otherwise specified, all used reagents were obtained from Sigma-Aldrich, Inc. (St. Louis, MO, USA); SDS-PAGE materials and ECL detection reagents were purchased from Bio-Rad Laboratories, (Hercules, USA); anti-Fbx32/Atrogin1 (ab168372), anti-OXPHOS (ab110413), anti-STAT3 (ab68153), and anti-Myosin Heavy Chain (MHC) (ab 91506) primary antibodies were from Abcam (Cambridge, UK); anti-PDH-E1 (sc-377092) and anti-ubiquitin (sc-8017) primary antibodies, mitochondrial pyruvate carrier (MPC) inhibitor UK5099 (sc-361394) and STAT3 inhibitor WP1066 (sc-203282) were from Santa Cruz Biotechnology (Dallas, TX, USA); anti-LC3B (#3868) and anti-phospho-Tyr705-STAT3 (#9145) primary antibodies were from Cell Signaling Technology Inc. (Danvers, MA,USA); Tetramethyl-rhodamine methyl ester (TMRM) probe was from Molecular Probe (Eugene, OR, USA); K-LATE kit for lactate assay was from Megazyme (Bray, Ireland); pyridine and N-tert-Butyldimethylsilyl-N-methyltrifluoroacetamide with 1% tert-Butyldimethylchlorosilane (MBTSTFA + 1% TBDMCS) were from Pierce, ThermoFisher Scientific (Waltham, MA, USA).

2.2 | Methods

2.2.1 | Cell culture

Murine C2C12 myoblasts and CT26 colon carcinoma cells were routinely grown in Dulbecco's modified Eagle's

medium (DMEM, #ECB7501 Euroclone, Milan, Italy) supplemented with 10% fetal bovine serum in a 5% CO_2 humidified atmosphere (growing medium). Myoblast differentiation into myotubes has been obtained by shifting sub-confluent C2C12 myoblasts to differentiating medium composed of DMEM containing 2% Horse Serum (HOS) for at least 4 days.

2.2.2 | Preparation of conditioned media (CM) and treatment

CT26 colon carcinoma cells were cultured until subconfluence. Cells were washed twice with PBS and then the medium was replaced with serum-free DMEM for 48 h. During this time, the culture medium became a conditioned medium (CM) from the secretory activity of CT26 tumor cells. Obtained CM CT26 was centrifuged at 1500 rpm to remove debris and immediately stocked at −80°C until used. For myotube treatment, CM CT26 was diluted at 20% final as reported.[15] Sodium pyruvate (20 mM final) was added to 20% CM CT26 and maintained throughout the experiment.

2.2.3 | Gas chromatography-mass spectrometry (GC–MS)

Gas chromatography-mass spectrometry (GC–MS) analysis of myotube intracellular metabolomic profile was performed using selected ion monitoring (SIM) mode MS. Myotubes were scraped in 80% methanol and phase separation was achieved by centrifugation at 4°C. The methanol-water phase containing polar metabolites was separated and dried using a vacuum concentrator. Dried polar metabolites were dissolved in 10 µl of 40 mg/ml methoxamine hydrochloride in pyridine (Pierce, ThermoFisher Scientific) and kept at 37°C for 2 h. After dissolution and reaction, 50 µl of MBTSTFA + 1% TBDMCS was added to the samples that were then incubated at 60°C for 1 h. Metabolite chromatographic separation was performed using Intuvo 9000 GC system equipped with HP-5MS UI (30 m × 250 µm × 0.25 µm) chromatographic capillary column (Agilent Technologies, Palo Alto, CA, USA) and coupled with 5977B MSD mass spectrometry system. Gas chromatography runs were performed with helium as carrier gas at 1.1 ml/min. The split inlet temperature was set to 250°C and the injection volume of 1 µl. The temperature of the GC oven was from 70 to 280°C. The first temperature ramp was from 70 to 140°C at 3°C/min. The second temperature ramp was from 140 to 150°C at 1°C/min. Finally, the last temperature ramp was from 150 to 280°C at 3°C/min. The data acquisition rate was 10 Hz. For the quadrupole, a source EI (70 eV) was used. The ion source and transfer line temperatures were set to 250 and 290°C, respectively. Using the SIM mode, characteristic ions for each analyte were used for peak identification and quantification (Table S1). For the determination of the relative abundances of metabolites, the integrated signal of all ions for each metabolite fragment was normalized on the total protein content of each sample.

2.2.4 | Immunoblot analysis

Cells were lysed for 10 min on ice in 100 µl of complete radio-immunoprecipitation assay (c-RIPA) buffer (150 mM NaCl, 100 mM NaF, 2 mM EGTA, 50 mM Tris HCl pH 7.5, 5 mM orthovanadate, 1% triton, 0.1% SDS, and 0.1% protease inhibitor cocktail). Clarified lysates were obtained by centrifugation at 14 000 rpm at 4°C for 10 min. The total protein content of each sample was obtained using the Bradford assay (Bio-Rad Laboratories, Hercules, USA). 10–20 µg of total proteins for each sample were separated by SDS-PAGE and transferred onto PVDF membranes. PVDF membranes were incubated with the target primary antibody in 2% non-fat dry milk solution (PBS, 0.05% tween) at 4°C for 24 h and with horseradish-conjugated secondary antibody for 1 h at room temperature. PVDF membranes were washed 3 times in washing solution (PBS, 0.1% tween) for 10 min and then a chemiluminescence reaction was achieved by probing PVDF membranes with ECL (Bio-Rad Laboratories, Hercules, USA). Target protein bands have been detected and analyzed using Amersham Imager 600 and ImageJ software, respectively. The expression level of the target protein was obtained using Coomassie-stained PVDF membranes for normalization.

2.2.5 | Oxygen consumption rate (OCR) analysis

After treatments, myotubes were detached and suspended in 1 ml of growing medium. The cell suspension was transferred to an airtight thermostatic chamber maintained at 37°C. Myotube oxygen consumption, measured by using a Clark-type O_2 electrode (Oxygraph Hansatech) for 10 min, has been achieved by taking the rate of oxygen consumption (nmol/min/ml) as an index of respiratory ability. The value of oxygen consumption rate (OCR) was normalized on the total protein content of each sample.

2.2.6 | PDH activity

PDH activity was assayed in cell lysates using PDH Activity Assay Kit (#MAK183, Sigma–Aldrich, St. Louis, USA). PDH activity (nmol/min/ml) was normalized on total protein content in each sample.

2.2.7 | Lactate assay

The lactate amount was assayed in a culture medium using the K-LATE kit (Megazyme, Bray, Ireland) according to the manufacturer's instructions. To obtain the amount of lactate produced exclusively from myotubes, the amount of lactate in CM CT26 was subtracted from the quantity of lactate in the medium of CM-treated myotubes. The values were normalized using total protein content in each sample.

2.2.8 | Confocal analysis

C2C12 myoblasts were grown to 80% confluence on glass coverslips and then differentiated for four days. The obtained myotubes were treated with CM CT26 with or without pyruvate for 24 h, washed in PBS, and immediately fixed in 4% paraformaldehyde at 4°C for 20 min. Subsequently, the membrane was washed three times with 50 mM Tris–HCl (pH 7.4), 150 mM NaCl, and 0.1% Triton X-100 (PBST) to obtain cell permeabilization, then the membrane was treated for 60 min with a blocking solution (5.5% horse serum in PBST). Coverslips with permeabilized cells were incubated with anti-MHC primary antibody (Abcam, Cambridge, UK) diluted 1:100 in PBST 3% BSA at 4°C for 24 h. Cells were firstly washed with PBST for 15 min and then with 0.1% BSA in PBST for 15 min. Coverslips were then incubated with secondary antibody (1:400) in PBST 3% BSA at room temperature for 1 h. For nuclei staining, cells were finally labeled with DAPI (250 nM final) at room temperature for 10 min. Analysis of mitochondrial membrane potential was performed by treating viable myotubes with a TMRM probe (40 nM final) at 37°C for 15 min and immediately observed using a confocal fluorescence microscope Leica TCS SP8 (Leica Microsystems, Germany).

2.2.9 | Electrophysiological analysis

The passive properties of myotubes have been assayed by the whole cell patch-clamp technique in voltage-clamp mode. For the electrophysiological records, the plate was placed in the proper chamber located on the stage of the Nikon Eclipse TE200 inverted microscope (Nikon Europe BV, 1076 ER Amsterdam, The Netherlands) and constantly superfused at a rate of 1.8 ml/min with the following physiological bath solution (mM):150 NaCl, 5 KCl, 2.5 $CaCl_2$, 1 $MgCl_2$, 10 D-glucose and 10 HEPES (pH 7.4 with NaOH). Patch pipettes were achieved from borosilicate glass capillaries (GC150-7.5, Harvard apparatus LTD) by a two-stage vertical puller (Narishige, Tokyo, Japan) and were filled with an internal solution (mM): 130 KCl, 10 NaH_2PO_4, 0.2 $CaCl_2$, 1 EGTA, 5 MgATP and 10 HEPES (pH 7.2). When filled, the patch pipette's resistance was 1.5–2 MΩ. The patch pipette was inserted in a CV203BU head-stage (Axon Instruments, Foster City, CA) attached to a three-way coarse manipulator and micromanipulator (Narishige, Tokyo, Japan) and an Axopatch 200 B amplifier (Axon Instruments, Foster City, CA) as previously described.[16] Voltage-clamp protocol generation and data acquisition were managed by the A/D-D/A interfaces (Digidata 1200; Axon Instruments) and Pclamp 6 software (Axon Instruments Foster City, CA). Starting from a holding potential (HP) of −70 mV, we applied a 10-mV negative and positive step pulse to evoke only the passive currents, consisting of an early capacitive transient (I_c) followed by a steady resistive current (I_r). The parameter C_m represents the cell linear capacitance and is used as an index of the cell surface, being the membrane-specific capacitance constant at 1 $\mu F\,cm^{-2}$. The membrane resistance (R_m) was calculated as already reported[17] and the membrane conductance $G_m = 1/R_m$ is indicative of membrane permeability. The ratio G_m/C_m is intended as specific conductance. Records were made at room temperature (22°C).

2.2.10 | Statistical analysis

Data are presented as mean ± SD from at least three independent experiments. Statistical analysis of the data was performed by Student's *t* test or by one-way ANOVA, using GraphPad Prism (Graphpad Holdings, LLC, USA), version 6.0. A *p*-value <.05 was considered statistically significant.

3 | RESULTS

3.1 | Metabolomic analysis of the cachectic myotubes

Recently, we described that cachectic myotubes display a metabolic change, upregulating lactate production and decreasing oxygen consumption.[15] To study in

depth what happened within cachectic myotubes, we performed intracellular metabolomic analysis, focusing on glycolysis and Krebs cycle metabolites. Metabolomic analysis shows decreased level of glucose-6 phosphate and increased amounts of both pyruvate and lactate in CM CT26-treated myotubes in comparison with control. These results are in agreement with our previous observations, showing enhanced glucose uptake and increased lactate production in cachectic myotubes.[15] Regarding Krebs cycle intermediates, CM CT26-treated myotubes display decreased amounts of citrate, succinate, and malate and enhanced α-ketoglutarate content, while fumarate level is unchanged compared to control myotubes (Figure 1).

In agreement with published results,[15] these findings demonstrate that glycolysis and lactic fermentation are up-regulated in cachectic myotubes.

3.2 | Sodium pyruvate impedes the development of the cachectic features in myotubes

We hypothesized that, upon cachexia induction, the majority of pyruvate in cachectic myotubes is driven toward lactic fermentation, with a little amount of the metabolite driven into mitochondria. Hence, we planned to analyze the effect of pyruvate addition on the onset of cachexia in myotubes. For this aim, sodium pyruvate (20 mM final) has been added to CM CT26 and used for treating myotubes for 24 h. Images of myotubes from a confocal microscope show that myotubes treated with CM CT26 containing sodium pyruvate display a phenotype similar to control myotubes (Figure 2A). A deeper analysis demonstrates that sodium pyruvate blocks the thinning of myotubes (Figure 2B), and the decrease in MHC level (as

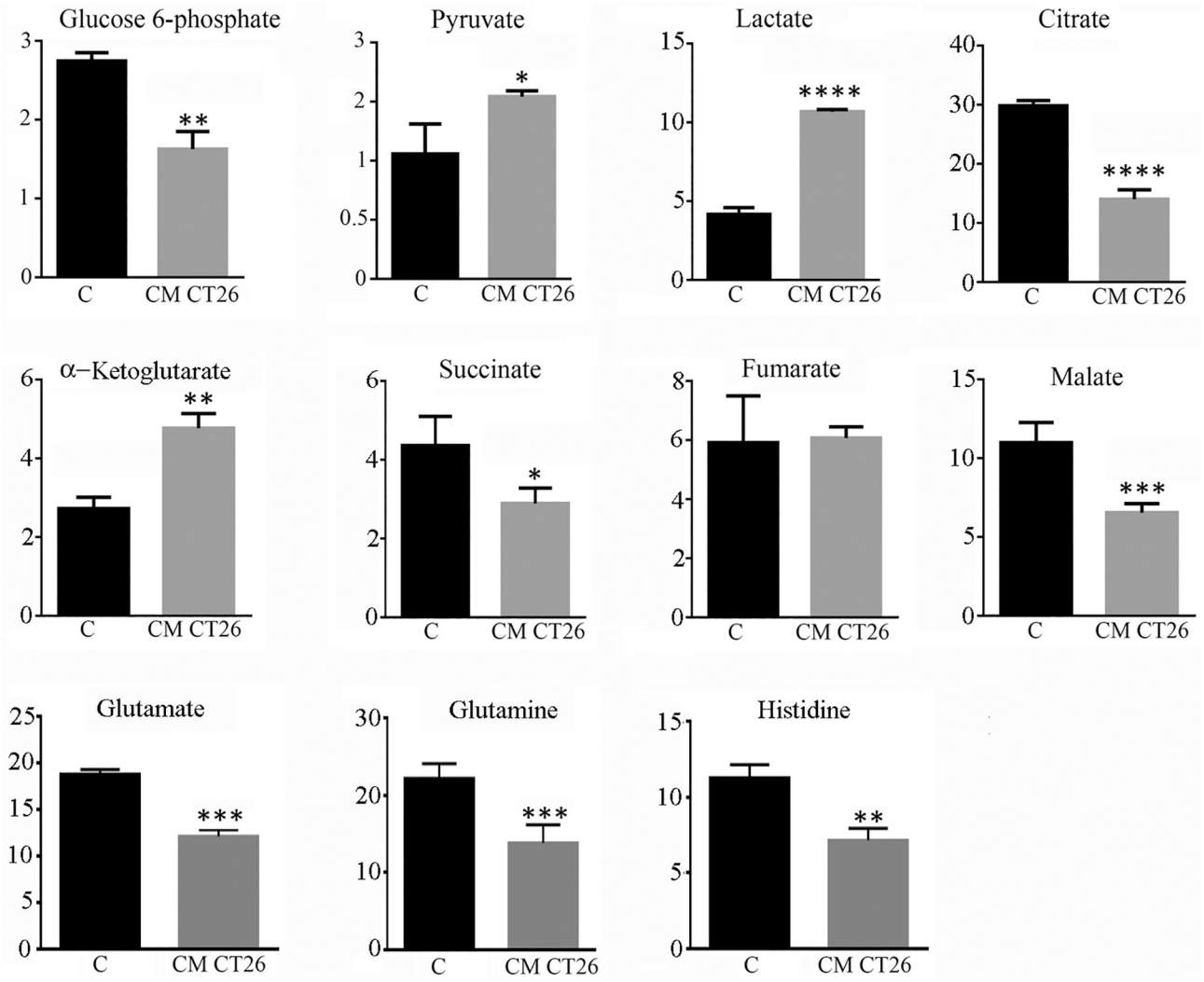

FIGURE 1 Intracellular metabolomics in control and CM CT26-treated myotubes. Bar graphs illustrate the level of the metabolites involved in glycolysis, Krebs cycle, and the amino acids fuelling the three carboxylic acid cycle. *$p < .05$, **$p < .005$, ***$p < .001$, ****$p < .0001$ vs. control (C). $n = 3$.

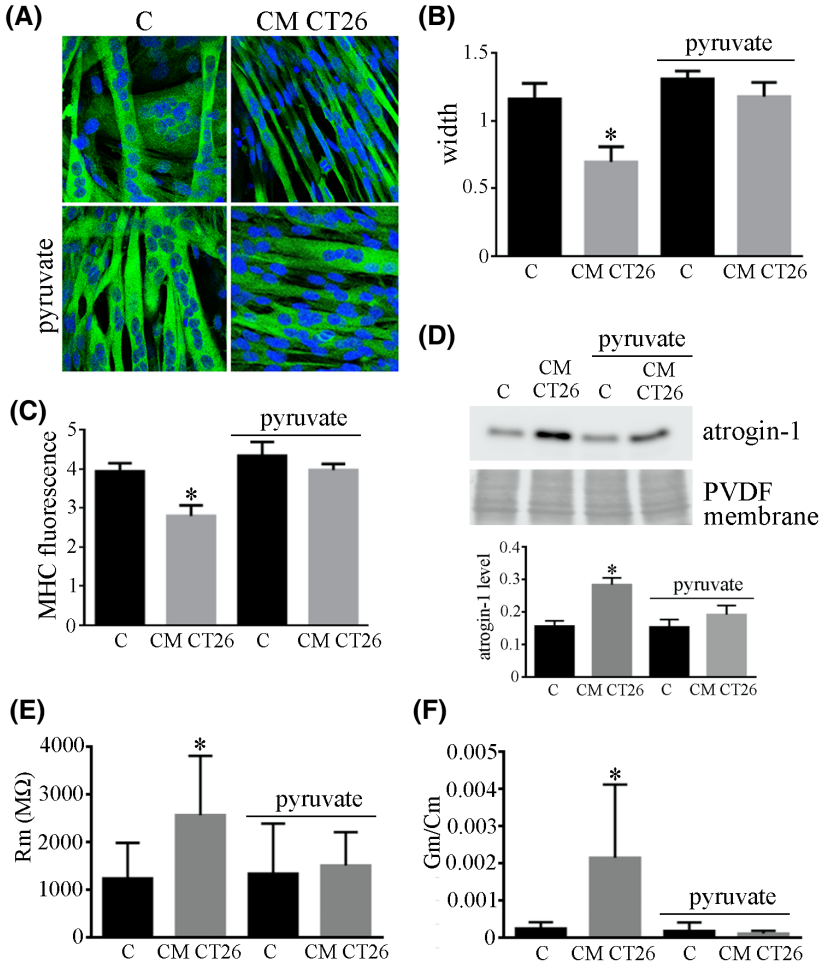

FIGURE 2 Sodium pyruvate prevents the acquisition of cachectic features in CM CT26-treated myotubes. Myotubes have been treated with CM CT26 for 24 h. Where indicated sodium pyruvate (20 mM final) was added to CM CT26. (A) Representative confocal images. MHC is shown by green fluorescence, while DAPI staining (blue fluorescence) evidences nuclei. (B) Myotube width measured in at least 10 randomly chosen fields using Image J software. The mean value for each sample has been reported in the bar graph. (C) MHC fluorescence. At least 10 randomly chosen fields are used to measure green fluorescence by Image J software and the mean value for each sample has been reported in the bar graph. (D) Anti-atrogin-1 immunoblot. The bar graph reports the atrogin-1 level in myotubes. $n = 4$; $^*p < .05$. (E) Analysis of membrane resistance (Rm). Rm values, measured as MΩ, in control myotubes, indicated as C, ($n = 37$), in CM CT26-treated myotubes ($n = 21$), in control myotubes containing sodium pyruvate ($n = 25$), and in CM CT26-treated myotubes containing sodium pyruvate ($n = 23$). $^*p < .05$ vs. C. (F) Analysis of membrane conductance (Gm/Cm). Gm/Cm values measured in control myotubes indicated as C ($n = 15$), in CM CT26-treated myotubes ($n = 11$), in control myotubes containing sodium pyruvate ($n = 15$) and in CM CT26-treated myotubes containing sodium pyruvate ($n = 11$). $^*p < .05$ vs. C.

shown by the green fluorescence measure) (Figure 2C), induced by CM CT26. Moreover, myotubes treated with CM CT26 containing pyruvate show decreased Atrogin-1 level, which appears up-regulated in CM CT26-treated myotubes in comparison to control myotubes (Figure 2D).

Moreover, we assayed whether sodium pyruvate could revert both phenotypic and metabolic features in cachectic myotubes. We observed that this treatment reverts the phenotype and the metabolism of diseased myotubes like control, as shown by myotube width (Figure S1A,B), MHC expression level (Figure S1C), lactate production (Figure S1E) and oxygen consumption (Figure S1F), thus demonstrating that this metabolite induces the reversion of a pre-existing cachectic condition. With regard to the electrophysiological passive properties of myotubes, the Rm values resulted significantly altered in myotubes treated with CM CT26 compared to control counterpart. Pyruvate addition in CM CT26-treated myotubes induced similar effects to those observed in the control condition, whereas myotubes treated with sodium pyruvate alone does not show alterations of membrane resistance (Figure 2E). This suggests that the significant modification of membrane permeability induced by the CM CT26 is hindered by the use of sodium pyruvate. Based on the observation that CM CT26-treated myotubes show smaller membrane capacitance than control ones, we normalized the

membrane conductance, G_m, (obtained from R_m values) with membrane capacitance, C_m. Interestingly, the mean G_m/C_m values resulted significantly increased in myotubes treated with CM CT26. The addition of sodium pyruvate to CM CT26 re-establishes G_m/C_m values comparable to those observed in control myotubes. This suggests that the clear alteration of membrane-specific conductance observed in the CM CT26 is effectively recovered by the use of sodium pyruvate (Figure 2F).

Collectively, these findings demonstrate that increasing sodium pyruvate concentration impedes the acquisition of cachectic features in myotubes treated with CM CT26.

3.3 | Sodium pyruvate blocks the metabolic shift induced by CM CT26 in myotubes

We then tested the influence of sodium pyruvate in the promotion of the metabolic change occurring in cachectic myotubes. Myotubes treated for 24 h with CM CT26 containing sodium pyruvate show a lactate production similar to that observed in control myotubes. In contrast and as expected, myotubes treated with CM CT26 without sodium pyruvate produce higher amounts of lactate compared to control cells (Figure 3A). At the mitochondrial level, the treatment of myotubes with CM CT26 induces the decrease of mitochondrial membrane potential, oxygen consumption, and OXPHOX level.[15] In contrast, the addition of sodium pyruvate to CM CT26 prevents the decrease of the oxygen consumption rate (Figure 3B), the depolarization of mitochondrial membrane (observed using the TMRM probe) (Figure 3C), and the reduction of OXPHOX levels (Figure 3D).

These observations demonstrate that the increase of sodium pyruvate concentration impedes the metabolic shift induced by CM CT26, hindering the appearance of the cachectic features in myotubes.

3.4 | PDH activity is unaffected in myotubes treated with CM CT26 containing sodium pyruvate

We believe that reactivation of PDH activity could be a key step for blocking the metabolic shift observed in myotubes following CM CT26 treatment, and for impeding the induction of the cachectic characters. Although metabolomic analysis shows high pyruvate amount in cachectic myotubes, the majority of this metabolite could be driven toward lactate formation, thus subtracting the substrate for PDH. Hence, we hypothesized that PDH activity could be recovered by adding sodium pyruvate to CM CT26. As expected, PDH activity is decreased in myotubes treated with CM CT26, while

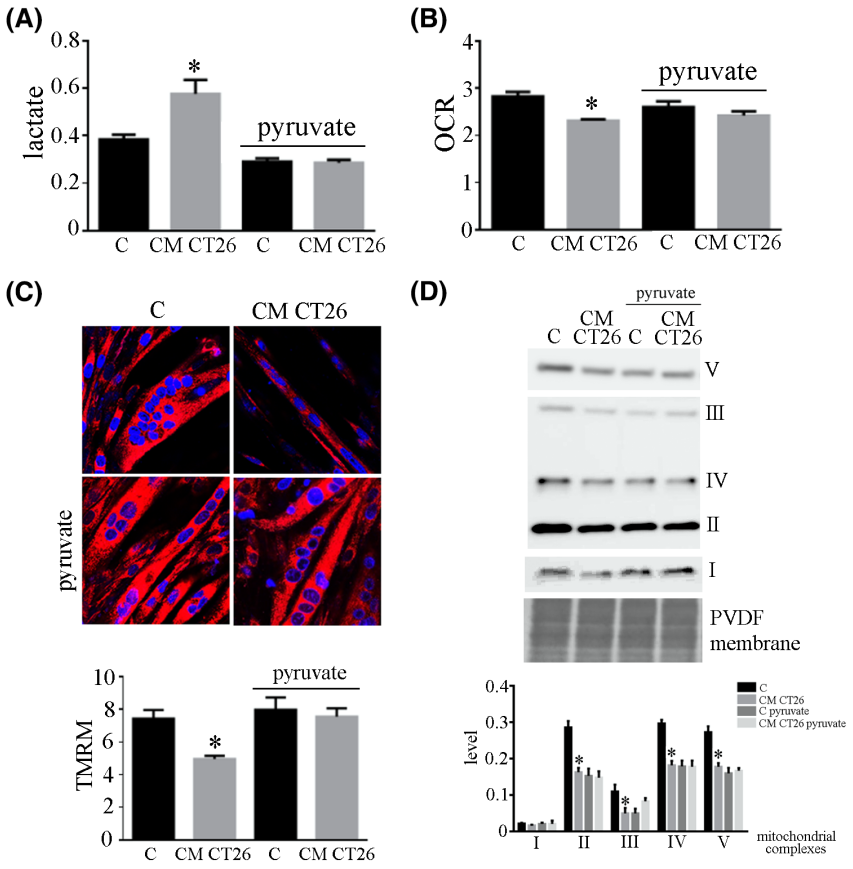

FIGURE 3 Sodium pyruvate impedes the shift toward lactic fermentation in CM CT26-treated myotubes. Myotubes have been treated with CM CT26 for 24 h. Where indicated sodium pyruvate (20 mM final) was added to CM CT26. (A) Lactate assay. (B) Oxygen Consumption Rate (OCR). (C) Representative confocal images of mitochondria. Mitochondria have been stained with TMRM probe (red fluorescence), while DAPI staining shows nuclei (blue fluorescence). TMRM fluorescence has been measured using Image J software in at least 10 randomly chosen fields and reported as the mean value in the bar graph. (D) Anti-OXPHOX immunoblot. Bar graph reports the level of each mitochondrial complex in myotubes. C, Control myotubes. $n = 3$; $^*p < .05$.

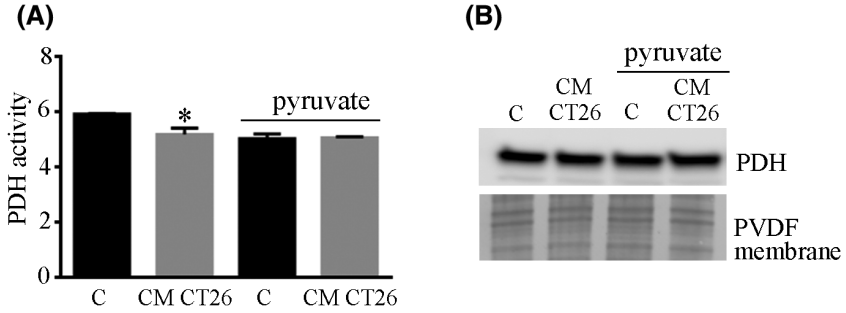

FIGURE 4 PDH activity is unaffected by CM CT26 in the presence of sodium pyruvate. Myotubes have been treated with CM CT26 for 24 h. Where indicated sodium pyruvate (20 mM final) was added to CM CT26. (A) PDH activity. (B) Anti-PDH immunoblot. C, control myotubes. $n = 4$; $^*p < .05$.

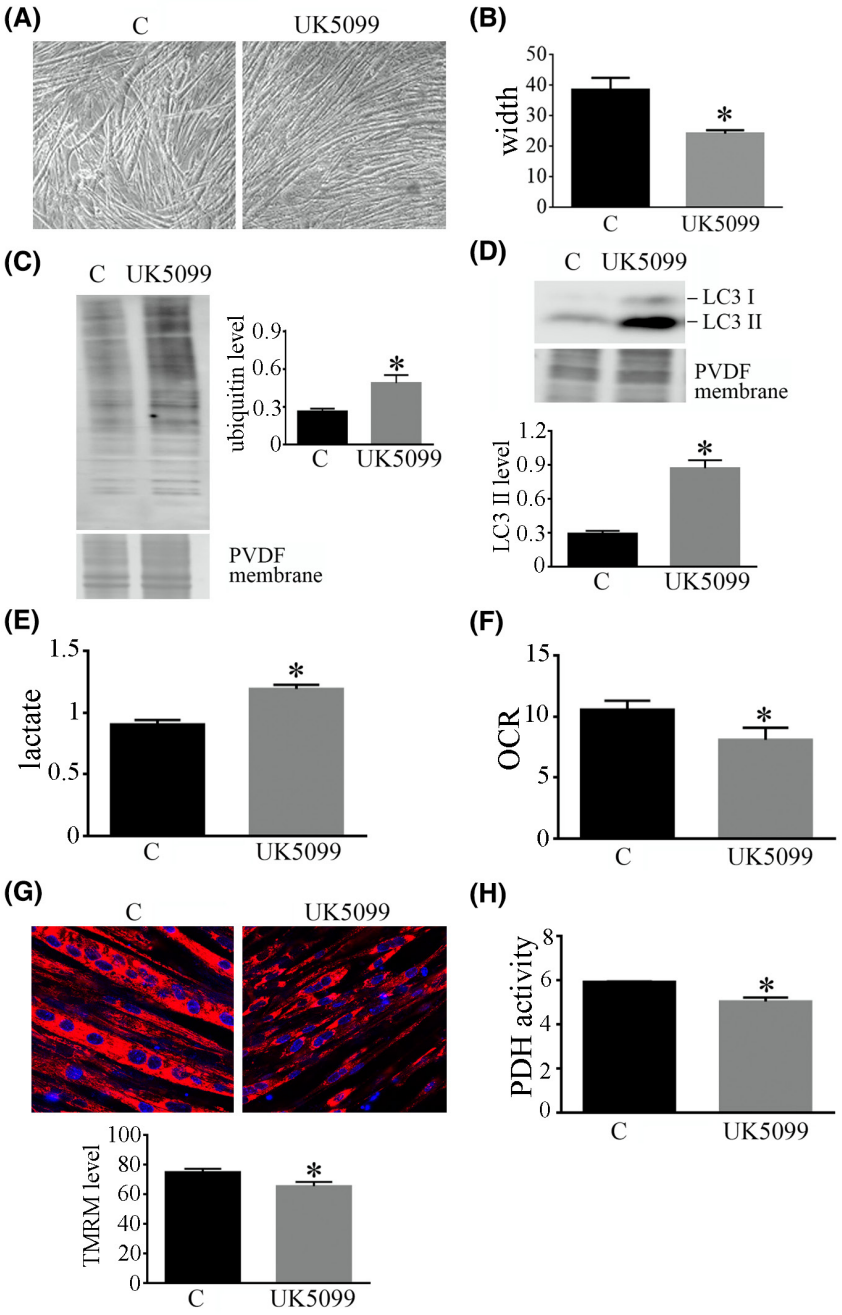

FIGURE 5 Myotubes treated with the MPC inhibitor UK5099 acquire cachectic features. Myotubes have been treated with UK5099 (10 μM final) for 24 h. (A) Representative images of control and UK5099-treated myotubes. (B) Myotube width obtained by ImageJ and calculated in at least 10 randomly chosen fields. (C) Ubiquitin immunoblot. (D) LC3II immunoblot. In (C) and (D) the bar graph reports the mean value of each sample obtained by the ratio with the PVDF membrane used for normalization. (E) Lactate assay. (F) Oxygen consumption rate (OCR). (G) Analysis of mitochondrial membrane potential by confocal microscopy. Mitochondria are stained with TMRM probe (red fluorescence), while blue fluorescence shows the nuclei. The bar graph reports the mean value of fluorescence for each sample measured using ImageJ software in at least 10 randomly chosen fields. (H) PDH activity. C, control myotubes. $n = 3$; $^*p < .05$.

the addition of sodium pyruvate actually hamp the decrease of PDH activity (Figure 4A). At the same time, PDH expression level is not affected by any treatment (Figure 4B).

3.5 | Inhibition of the mitochondrial pyruvate carrier is sufficient to induce cachectic features in myotubes

To investigate the role of the mitochondrial pyruvate flux in the induction of cachexia, myotubes have been treated with the mitochondrial pyruvate carrier (MPC) inhibitor UK5099. Then, the acquisition of the cachectic features, as well as the metabolic modifications, have been tested in UK5099-treated myotubes. We observed that the treatment of myotubes with UK5099 (10 μM final) for 24 h, induces the acquisition of cachectic phenotype in myotubes, as demonstrated by the thinning of their width (Figure 5A,B) and the activation of the ubiquitin (Figure 5C) and autophagic pathways (Figure 5D). As regards metabolism, the UK5099 treatment provokes metabolic modifications similar to those induced by CM CT26, namely an increased lactate production (Figure 5E) and a decreased oxygen consumption (Figure 5F). Moreover, UK5099 treatment provokes the decrease of mitochondrial membrane potential (Figure 5G) associated to the reduction of PDH activity (Figure 5H).

These results show that mitochondrial pyruvate deprivation is involved in cachectic feature development, highlighting the importance of a suitable mitochondrial pyruvate amount to counteract cachexia induction in myotubes.

3.6 | Sodium pyruvate addition impedes the activation of the STAT3 pathway due CM CT26 treatment

We analyzed STAT3 phosphorylation in CM CT26-treated myotubes and how the addition of sodium pyruvate can

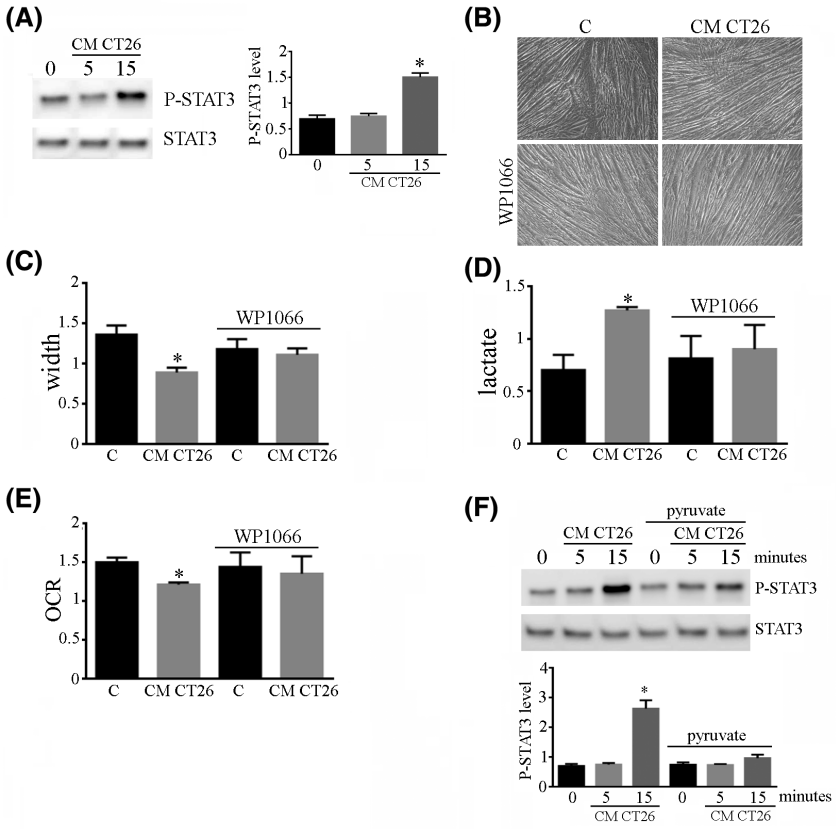

FIGURE 6 STAT3 signaling pathway. (A) Myotubes have been stimulated with CM CT26 for the indicated period and STAT3 phosphorylation (Tyr705) has been analyzed by immunoblot. The bar graph shows the STAT3 phosphorylated level on Tyr705. Myotubes have been treated with CM CT26 for 24 h. Where indicated, the STAT3 inhibitor WP1066 (10 μM) has been added to CM CT26 along the experiment. (B) Representative images of myotubes. (C) Myotube width measured using Image J software in at least 10 randomly chosen fields. The mean value for each sample has been reported in the bar graph. (D) Lactate assay. (E) Oxygen consumption rate (OCR). (F) Myotubes have been stimulated with CM CT26 for the indicated period. Sodium pyruvate (20 mM final) has been added 30 min before the treatment with CM CT26. STAT3 phosphorylation (Tyr705) has been analyzed by immunoblot. The bar graph shows the STAT3 phosphorylated level on Tyr705. C, control myotubes. $n = 4$; $^*p < .05$.

affect the activation of this pathway. We observed that CM CT26 induces high STAT3 phosphorylation (Figure 6A). To study the effective involvement of STAT3 signaling in the induction of cachexia, the STAT3 inhibitor WP1066 has been added to CM CT26. The inhibition of the STAT3 pathway actually impedes the onset of cachectic features since myotubes show width (Figure 6B,C), as well as lactate production (Figure 6D) and OCR consumption (Figure 6E) like control cells (Figure 6B,C), strongly suggesting that the activation of STAT3 pathway is engaged in the CM Ct26-induced cachexia. Notably, addition of sodium pyruvate decreases STAT3 phosphorylation (Figure 6F), thus blocking the cachexia onset induced by CM CT26. Decreased STAT3 phosphorylation is also observed when sodium pyruvate is added to pre-existing cachectic myotubes, demonstrating that the rescue of a normal phenotype and metabolism is driven by STAT3 signaling (Figure S2).

Overall, these observations strongly demonstrate that STAT3 signaling is significantly involved in the CM CT26-induced cachexia and that sodium pyruvate impairs the activation of this signaling cascade.

4 | DISCUSSION

This paper shows that enhanced pyruvate concentration prevents the acquisition of both phenotypic and metabolic cachectic features in myotubes. In particular, the sodium pyruvate addition to CM CT26 prevents the thinning of myotubes and the metabolic alterations important for cancer cachexia onset. In our previous paper, we demonstrated that the appearance of the cachectic features in myotubes is strictly associated with a metabolic shift toward lactic fermentation. Namely, cachectic myotubes increase lactate production and decrease oxygen consumption. Interestingly, when this metabolic alteration is impeded, by inhibiting glycolysis with 2-deoxyglucose or by decreasing lactate dehydrogenase activity with oxamate, the appearance of the cachectic features is hampered. This observation certainly highlights the key role of such metabolic alterations in cachexia onset.[15] It is abundantly reported that cancer cachexia is associated with several metabolic changes.[18,19] Our research group previously reported that cachectic myotubes show enhanced glucose uptake.[15] Our metabolomic data confirm that CM CT26-treated myotubes show enhanced glycolysis, as demonstrated by increased pyruvate production, and increased lactate formation. On the contrary, citrate, the first product of the Krebs cycle is greatly reduced in CM CT26-treated myotubes, thus suggesting an impairment of the tricarboxylic acid cycle. The high level of alpha-ketoglutarate observed in cachectic myotubes could be due to anaplerotic reactions, using glutamate, glutamine, or histidine as substrates, aimed at fuelling the Krebs cycle. In agreement, glutamate, glutamine, and histidine amounts are decreased in cachectic myotubes in comparison to the control counterpart.

Increased lactate amount suggests that the majority of pyruvate produced by glycolysis is converted into lactate, and only a small amount enters in the mitochondria. Pyruvate comes into mitochondria by means of MPCs (MCP1 and MCP2 in mammals), integral mitochondrial inner membrane proteins[20] that carry pyruvate through a proton symport mechanism.[21] An adequate entry of pyruvate in mitochondria could regulate cell metabolism, while its inhibition promotes metabolic modifications. As well, the cytosolic pyruvate concentration can influence MPC activity, since a rise in the cytosolic pyruvate concentration prevents the conversion of pyruvate to lactate.[22] Moreover, MCP destruction in mice leads to enhanced glucose uptake and lactate extrusion[23] in muscle and to increased glutaminolysis to produce Krebs cycle intermediates.[24] Here, we demonstrate the importance of MPC involvement in metabolism and phenotypic modifications by treating the myotubes with the MPC inhibitor UK5099. This molecule covalently binds to MPC and blocks pyruvate transport.[25] Our results demonstrate that MPC inhibition leads to the acquisition of phenotypic features typical of cachexia associated with metabolic modifications, thus highlighting the key role of the pyruvate flux in mitochondria.

Within mitochondria, pyruvate can be used as a substrate by pyruvate carboxylase or pyruvate dehydrogenase (PDH), the latter belonging to the Pyruvate Dehydrogenase Complex (PDC). PDC catalyzes the irreversible conversion of pyruvate into Acetyl-CoA, which is used in the first reaction of the Krebs cycle.[7] PDC consists of three subunits called E1, E2, and E3. Among these, the E1 subunit, that corresponds to PDH, catalyzes the first reaction of PDC, leading to the decarboxylation of pyruvate.[26] PDC activity is controlled by the PDH phosphorylation level. Pyruvate dehydrogenase kinases (PDKs) induce PDH phosphorylation on specific serine residues, thus inducing PDH inactivation.[27] Several metabolites regulate PDKs activity, being activated by the high $NADH^+H^+/NAD^+$ and Acetyl-CoA/CoA ratio, and inhibited by pyruvate through an allosteric mechanism.[28] Particularly, PDK4 exerts a role in muscle wasting both in C2C12 cultures and cachectic mice. Increased PDK4 activity, obtained through pharmacological treatment with WY-14643 (an agonist for the PPAR-α) or by PDK4 overexpression, leads to muscle wasting in myotubes.[8] Moreover, decreased PDH activity has been shown both in myotubes and in the muscles of cachectic mice.[8,15] Based on the role of PDH in cancer cachexia onset, we hypothesized that PDH activity could be

restored by enhancing the enzyme substrate. This could lead to the formation of Acetyl-CoA by the PDC, while a smaller amount of pyruvate can be used by the LDH. In agreement with this hypothesis, we found that the increase in pyruvate amount in the culture media abundantly inhibits the formation of cachectic myotubes, both for the acquisition of the cachectic phenotype and for the metabolic modifications.

Our data clearly indicate that PDH activity remains similar to control myotubes, thus suggesting that PDH reactivation could be a crucial point in cachexia onset and sodium pyruvate addition could be a modality to reach this aim. Moreover, mitochondria undergo several disorders in cachectic conditions, ranging from membrane depolarization, decrease of OXPHOS level, and reduction of oxygen consumption.[29–32] In agreement with the results on PDH, we found that pyruvate addition impedes the acquisition of these modifications in mitochondria.

Regarding passive properties of membrane myotube, our results support an effect of CM CT26 in inducing an increase in specific membrane conductance. This outcome is in agreement with previous observations on atrophic myotubes made by our research group. Indeed, atrophic myotubes showed an increased membrane permeability and a reduction of cell capacitance.[16] Here, we demonstrate that the presence of sodium pyruvate in CM CT26 counteracted the occurence of these alterations, showing membrane parameters similar to untreated myotubes.

The signal transducer and activator of transcription 3 (STAT3) signaling pathway is greatly involved in the development of muscle atrophy during cancer cachexia. STAT3 activation is known to induce the enhanced expression of MAFbx/Atrogin-1 and the ubiquitin-proteasome system, thus promoting cachexia.[13,33–35] Conversely, the blockade of STAT3 signaling suppresses cancer cachexia both in vitro and in vivo.[36] In the present study, we reported that CM CT26 induces STAT3 phosphorylation and the inhibition of the STAT3 signaling, achieved by using WP1066, prevents the formation of cachectic features, such as the thinning of myotubes and the metabolic modifications. Indeed, the myotubes treated with the STAT3 inhibitor show lactate production and oxygen consumption similar to control myotubes. Our results show that pyruvate added to CM CT26 prevents the formation of cachectic myotubes through the downregulation of the STAT3 signaling pathway. Figure 7 shows the effects induced by pyruvate on CM CT26-treated myotubes.

Our study highlights the importance of the adequate amount of mitochondrial pyruvate for the maintenance of normal phenotype and metabolism. The decrease of this metabolite in mitochondria for example through MPC block, can lead to the inhibition of crucial metabolic

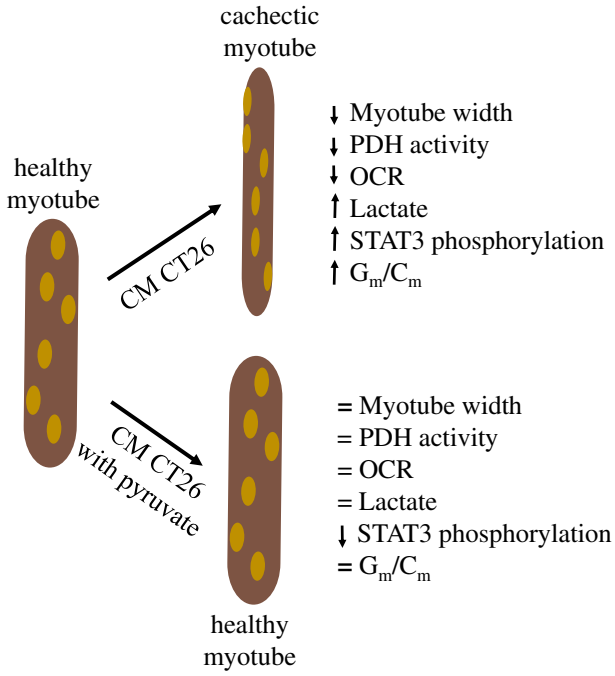

FIGURE 7 Effects of pyruvate in myotubes. The scheme summarizes the main features of cachectic myotubes and the effect of pyruvate addition to CM CT26. The arrows indicate the trend compared to the healthy myotubes (up arrow, increase; down arrow, decrease; equal sign, no change).

enzymes, such as PDH, involved in the occurrence of the cachectic features. On the basis of our results, we suggest that pyruvate could be a new tool to counteract the development of cancer cachexia in myotubes. Enhanced pyruvate amount leads to PDH reactivation and to the block of metabolic changes that predispose to cachexia onset. We speculate that an increased pyruvate amount could force PDH reaction towards the formation of Acetyl-coA and decrease the substrate for LDH. Moreover, pyruvate can act as an allosteric inhibitor of PDK4 activity, that does not induce the PDH inhibitory phosphorylation. Although these results arise from an in vitro study, they highlight the identification of a metabolite, namely pyruvate, as a new target to counteract cancer cachexia. However, deeper studies will be necessary for a possible translation of this knowledge on cachectic patients. Future studies will be focused on the prevention of mitochondrial pyruvate decrease. For example, in vivo studies could be achieved on cachectic mice fed with a pyruvate rich diet. Moreover, the involvement of other metabolites in the induction of cancer cachexia could be investigated. Among these, lactate, whose production is considerably increased in cachectic myotubes, could play a prominent role in the onset of the pathology, thus deserving further in-depth study.

AUTHOR CONTRIBUTIONS

Tania Fiaschi conceived and designed the research; Michele Mannelli, Tania Gamberi, Francesca Magherini, and Rachele Garella performed the research and acquired the data; Roberta Squecco and Tania Fiaschi analyzed and interpreted the data. All authors were involved in drafting and revising the manuscript.

ACKNOWLEDGMENTS

This work was supported by the Italian Ministry of University and Research (MIUR). The authors thank Fondazione Italiana per la Ricerca sul Cancro (AIRC) for a one-year Fellowship (Project Code:IG- 25012). Open Access Funding provided by Universita degli Studi di Firenze within the CRUI-CARE Agreement.

DISCLOSURES

The authors declare no conflicts of interest.

DATA AVAILABILITY STATEMENT

Data sharing is not applicable to this article as no datasets were generated or analyzed during the current study.

ORCID

Tania Fiaschi https://orcid.org/0000-0001-7321-3849

REFERENCES

1. Fearon K, Arends J, Baracos V. Understanding the mechanisms and treatment options in cancer cachexia. *Nat Rev Clin Oncol*. 2013;10:90-99.
2. Fearon KC, Glass DJ, Guttridge DC. Cancer cachexia: mediators, signaling, and metabolic pathways. *Cell Metab*. 2012;16:153-166.
3. Argilés JM, López-Soriano FJ. The ubiquitin-dependent proteolytic pathway in skeletal muscle: its role in pathological states. *Trends Pharmacol Sci*. 1996;17:223-226.
4. Bilodeau PA, Coyne ES, Wing SS. The ubiquitin proteasome system in atrophying skeletal muscle: roles and regulation. *Am J Physiol Cell Physiol*. 2016;311:C392-C403.
5. Bodine SC, Baehr LM. Skeletal muscle atrophy and the E3 ubiquitin ligases MuRF1 and MAFbx/atrogin-1. *Am J Physiol Endocrinol Metab*. 2014;307:E469-E484.
6. Pin F, Barreto R, Couch ME, Bonetto A, O'Connell TM. Cachexia induced by cancer and chemotherapy yield distinct perturbations to energy metabolism. *J Cachexia Sarcopenia Muscle*. 2019;10:140-154.
7. Patel MS, Korotchkina LG. Regulation of the pyruvate dehydrogenase complex. *Biochem Soc Trans*. 2006;34:217-222.
8. Pin F, Novinger LJ, Huot JR, et al. PDK4 drives metabolic alterations and muscle atrophy in cancer cachexia. *FASEB J*. 2019;33:7778-7790.
9. Wada E, Tanihata J, Iwamura A, Takeda S, Hayashi YK, Matsuda R. Treatment with the anti-IL-6 receptor antibody attenuates muscular dystrophy via promoting skeletal muscle regeneration in dystrophin−/utrophin-deficient mice. *Skelet Muscle*. 2017;7:23.
10. Zimmers TA, Fishel ML, Bonetto A. STAT3 in the systemic inflammation of cancer cachexia. *Semin Cell Dev Biol*. 2016;54:28-41.
11. Nunes AM, Wuebbles RD, Sarathy A, et al. Impaired fetal muscle development and JAK-STAT activation mark disease onset and progression in a mouse model for merosin-deficient congenital muscular dystrophy. *Hum Mol Genet*. 2017;26:2018-2033.
12. Ma JF, Sanchez BJ, Hall DT, et al. STAT3 promotes IFNγ/TNFα-induced muscle wasting in an NF-κB-dependent and IL-6-independent manner. *EMBO Mol Med*. 2017;9:622-637.
13. Ying L, Yao Y, Lv H, et al. IL-17A contributes to skeletal muscle atrophy in lung cancer-induced cachexia via JAK2/STAT3 pathway. *Am J Physiol Cell Physiol*. 2022;322:C814-C824.
14. Shukla SK, Markov SD, Attri KS, et al. Macrophages potentiate STAT3 signaling in skeletal muscles and regulate pancreatic cancer cachexia. *Cancer Lett*. 2020;484:29-39.
15. Mannelli M, Gamberi T, Magherini F, Fiaschi T. A metabolic change towards fermentation drives cancer cachexia in myotubes. *Biomedicine*. 2021;9:698.
16. Bernacchioni C, Squecco R, Gamberi T, et al. S1P signalling axis is necessary for adiponectin-directed regulation of electrophysiological properties and oxidative metabolism in C2C12 myotubes. *Cell*. 2022;11:713.
17. Martella D, Mannelli M, Squecco R, et al. Cell instructive liquid crystalline networks for myotube formation. *iScience*. 2021;24:103077.
18. Der-Torossian H, Wysong A, Shadfar S, Willis MS, McDunn J, Couch ME. Metabolic derangements in the gastrocnemius and the effect of compound a therapy in a murine model of cancer cachexia. *J Cachexia Sarcopenia Muscle*. 2013;4:145-155.
19. Porporato PE. Understanding cachexia as a cancer metabolism syndrome. *Oncogenesis*. 2016;5:e200.
20. Bricker DK, Taylor EB, Schell JC, et al. A mitochondrial pyruvate carrier required for pyruvate uptake in yeast, drosophila, and humans. *Science*. 2012;337:96-100.
21. Papa S, Francavilla A, Paradies G, Meduri B. The transport of pyruvate in rat liver mitochondria. *FEBS Lett*. 1971;12:285-288.
22. Du J, Cleghorn WM, Contreras L, et al. Inhibition of mitochondrial pyruvate transport by zaprinast causes massive accumulation of aspartate at the expense of glutamate in the retina. *J Biol Chem*. 2013;288:36129-36140.
23. Sharma A, Oonthonpan L, Sheldon RD, et al. Impaired skeletal muscle mitochondrial pyruvate uptake rewires glucose metabolism to drive whole-body leanness. *eLife*. 2019;8:e45873.
24. Vacanti NM, Divakaruni AS, Green CR, et al. Regulation of substrate utilization by the mitochondrial pyruvate carrier. *Mol Cell*. 2014;56:425-435.
25. Hildyard JC, Ammälä C, Dukes ID, Thomson SA, Halestrap AP. Identification and characterisation of a new class of highly specific and potent inhibitors of the mitochondrial pyruvate carrier. *Biochim Biophys Acta*. 2005;1707:221-230.
26. Sgrignani J, Chen J, Alimonti A, Cavalli A. How phosphorylation influences E1 subunit pyruvate dehydrogenase: a computational study. *Sci Rep*. 2018;8:14683.
27. Harris RA, Bowker-Kinley MM, Huang B, Wu P. Regulation of the activity of the pyruvate dehydrogenase complex. *Adv Enzyme Regul*. 2002;42:249-259.

28. Anwar S, Shamsi A, Mohammad T, Islam A, Hassan MI. Targeting pyruvate dehydrogenase kinase signaling in the development of effective cancer therapy. *Biochim Biophys Acta Rev Cancer*. 2021;1876:188568.
29. Tzika AA, Fontes-Oliveira CC, Shestov AA, et al. Skeletal muscle mitochondrial uncoupling in a murine cancer cachexia model. *Int J Oncol*. 2013;43:886-894.
30. Fontes-Oliveira CC, Busquets S, Toledo M, et al. Mitochondrial and sarcoplasmic reticulum abnormalities in cancer cachexia: altered energetic efficiency? *Biochim Biophys Acta*. 2013;1830:2770-2778.
31. Penna F, Ballarò R, Martinez-Cristobal P, et al. Autophagy exacerbates muscle wasting in cancer cachexia and impairs mitochondrial function. *J Mol Biol*. 2019;431:2674-2686.
32. Fermoselle C, García-Arumí E, Puig-Vilanova E, et al. Mitochondrial dysfunction and therapeutic approaches in respiratory and limb muscles of cancer cachectic mice. *Exp Physiol*. 2013;98:1349-1365.
33. Hu W, Ru Z, Zhou Y, et al. Lung cancer-derived extracellular vesicles induced myotube atrophy and adipocyte lipolysis via the extracellular IL-6-mediated STAT3 pathway. *Biochim Biophys Acta Mol Cell Biol Lipids*. 2019;1864:1091-1102.
34. Silva KA, Dong J, Dong Y, et al. Inhibition of Stat3 activation suppresses caspase-3 and the ubiquitin-proteasome system, leading to preservation of muscle mass in cancer cachexia. *J Biol Chem*. 2015;290:11177-11187.
35. Bonetto A, Aydogdu T, Jin X, et al. JAK/STAT3 pathway inhibition blocks skeletal muscle wasting downstream of IL-6 and in experimental cancer cachexia. *Am J Physiol Endocrinol Metab*. 2012;303:E410-E421.
36. Miller A, McLeod L, Alhayyani S, et al. Blockade of the IL-6 trans-signalling/STAT3 axis suppresses cachexia in Kras-induced lung adenocarcinoma. *Oncogene*. 2017;36:3059-3066.

SUPPORTING INFORMATION

Additional supporting information can be found online in the Supporting Information section at the end of this article.

How to cite this article: Mannelli M, Gamberi T, Garella R, Magherini F, Squecco R, Fiaschi T. Pyruvate prevents the onset of the cachectic features and metabolic alterations in myotubes downregulating STAT3 signaling. *The FASEB Journal*. 2022;36:e22598. doi:10.1096/fj.202200848R